The Journal of Toxicological Sciences (J. Toxicol. Sci.)
Vol.38, No.3, ***-***, 2013

Toxicomics Report

Comparative gene expression analysis of the amygdala in autistic rat models produced by pre- and post-natal exposures to valproic acid

Atsuko Oguchi-Katayama[1], Akihiko Monma[2], Yuko Sekino[1], Toru Moriguchi[2] and Kaoru Sato[1]

[1]Laboratory of Neuropharmacology, Division of Pharmacology, National Institute of Health Sciences, 1-18-1 Kamiyoga, Setagaya-ku, Tokyo 158-8501, Japan
[2]Department of Food and Life Sciences, Azabu University, 1-17-71 Fuchinobe, Tyuoku, Sagamihara-shi, Kanagawa 252-5201, Japan

(Received October 24, 2012; Accepted March 14, 2013)

ABSTRACT — Gene expression profiles in the amygdala of juvenile rats were compared between the two autistic rat models for mechanistic insights into impaired social behavior and enhanced anxiety in autism. The rats exposed to VPA by intraperitoneal administration to their dams at embryonic day (E) 12 were used as a model for autism (E2IP), and those by subcutaneous administration at postnatal day (P) 14 (P14SC) were used as a model for regressive autism; both of the models show impaired social behavior and enhanced anxiety as symptoms. Gene expression profiles in the amygdala of the rats (E12IP and P14SC) were analyzed by microarray and compared to each other. Only two genes, Neu2 and Mt2a, showed significant changes in the same direction in both of the rat models, and there were little similarities in the overall gene expression profiles between them. It was considered that gene expression changes per se in the amygdala might be an important cause for impaired social behavior and enhanced anxiety, rather than expression changes of particular genes.

Key words: Valproic acid, Amygdala, Microarray, Prenatal, Postnatal

INTRODUCTION

There are two similar but different kinds of autistic animal models produced by perinatal exposure of rodents to valproic acid (VPA). Rodents exposed to VPA on embryonic day (E) 12 have been used as an animal model for autism characterized by impaired social behavior, enhanced anxiety, and decreased sensitivity to pain after maturation (Markram *et al.*, 2008; Schneider and Przewtocki, 2005; Schneider *et al.*, 2007, 2008). On the other hand, rodents exposed to VPA on postnatal day (P) 14 have been used as an animal model for regressive autism that shows impaired social behavior like animal models for autism but accompanied by loss of some acquired skills (Yochum *et al.*, 2008, 2010; Wagner *et al.*, 2006). The regressive autism model also showed enhanced anxiety in our preliminary study.

The amygdala has been considered critical for behaviors associated with emotional disorders. Possible mechanisms of impaired social behavior in autism involve neural networks including the amygdala (Neuhaus *et al.*, 2010). The amygdala has also been identified to be involved in anxiety behaviors (Blackford and Pine, 2012). In humans, the amygdala and prefrontal cortex is the responsible for anxiety disorders (Etkin and Wager, 2007). It is therefore expected that comparative analysis of the amygdala in the two animal models for autism provide some mechanistic insights into impaired social behavior and enhanced anxiety in autism from similarities between them.

In the present study, we performed comparative gene expression analysis of the amygdala and characterize the similarities between the animal models for autism and for regressive autism. We first confirmed the effect of postnatal exposure to VPA on anxiety-related behavior in rats. We then compared gene expression profiles in the amygdala of juvenile rats between prenatal and postnatal exposures to VPA.

Correspondence: Kaoru Sato (E-mail: kasato@nihs.go.jp)

MATERIALS AND METHODS

Animals and VPA treatment

Pregnant Wistar Hannover/Rcc rats were obtained from Japan SLC, Inc. (Shizuoka, Japan) and maintained individually under conventional conditions with controlled temperature (23 ± 3°C) and illumination (12 hr; 7:00-19:00). Each of five litters was culled to 10 pups/litter on day 2 after birth for matched nursing conditions. For postnatal exposure, saline or 400 mg/kg of VPA (Sigma, St. Louis, MO, USA) was administered subcutaneously (s.c.) to half of the pups in each litter on postnatal day 14 (P14SC). For prenatal exposure, saline or 600 mg/kg of VPA was administered intraperitoneally (i.p.) to five pregnant rats on E12 (E12IP). Microarray analysis was performed at 5 (E12IP and P14SC) or 7 (P14SC7w) wks after the VPA administrations (Fig. 1). All animal treatments and experimental protocols were approved by the Animal Care and Use Committee of the Azabu University and the National Institute of Health Science (NIHS), and followed the Guide for the Care and Use of Laboratory Animals.

Behavioral test for anxiety

As a behavioral test, elevated plus maze (EPM) was performed in P14SC at 5 wks old with a maze consists of two opposite open arms (50 × 10 cm) and two opposite enclosed arms. The arms are connected by a central 10-cm square, forming a plus shape. The maze was elevated 50 cm above the floor. The animal's path was observed for 5 min after a resting period of 2 min in the central square of the maze. The number of entries into the open arms and the time spent in the open arms were measured.

Microarray analysis

Microarray analysis was performed using animals different from those used for behavioral test. The amygdalae were removed from the juvenile rats, and incubated in a RNA stabilization solution (RNAlater, Ambion, Austin, TX, USA) (1 ml for 5 x 5 x 5 (mm) block) overnight. Total RNA samples from the amygdalae were isolated with TRIzol (Invitrogen, Carlsbad, CA, USA) and the RNeasy Mini Kit (Qiagen, Hilden, Germany), with slight modifications to the manufacturer's protocol. The

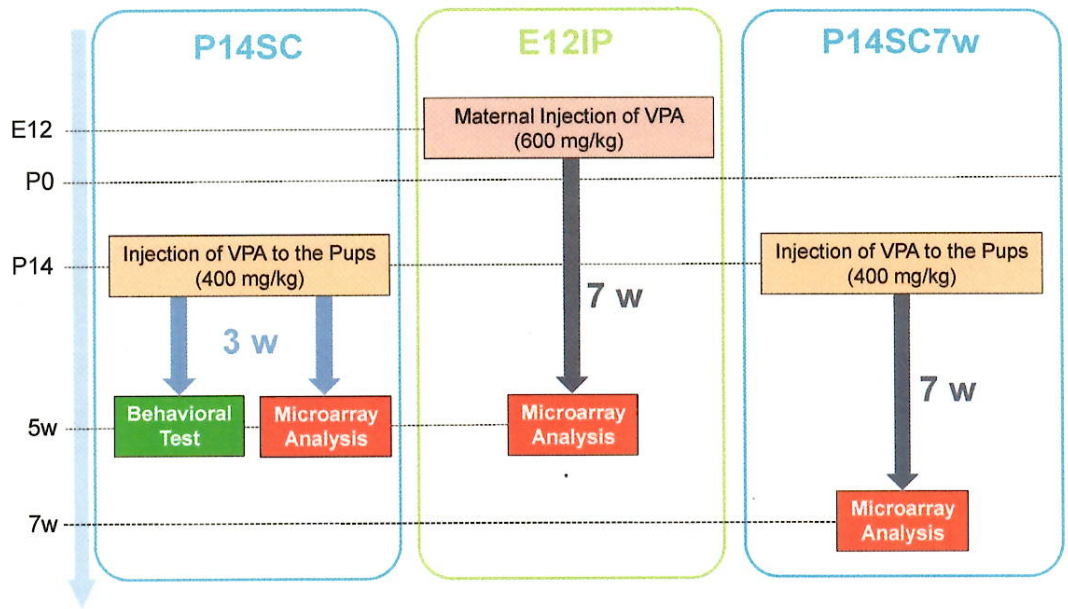

Fig. 1. The experimental design. To investigate the effect of postnatal VPA exposure on behavior and gene expression profiles, saline or 400 mg/kg VPA was administered to half of the pups per one litter subcutaneously on postnatal day 14 (P14SC). Behavior test and microarray analysis were performed using individual animals. To avoid influence of the dams, 5w juvenile rats (P35-37) were obtained evenly from 5 litters for control group and VPA- treated group, respectively. To investigate the effect of prenatal exposure, five pregnant rats were treated intraperitoneally (i.p.) with saline or 600 mg/kg VPA on E12.5 (E12IP), respectively, and microarray analysis was performed at 5w (P35-37). To analyze the contribution of the length of time from VPA exposure to cRNA isolation to the change in gene expression profile, microarray analysis was also performed at 7w (P49-56) (5 w after VPA exposure at P14) (P14SC7w).

isolated RNA sample (100 μg) were used for the microarray analysis (Affymetrix GeneChip Rat Genome 230 2.0 array (Santa Clara, CA, USA)) according to the Affymetrix protocol (http://www.affymetrix.com/support/technical/manuals.affx). Data were collected using Affymetrix GeneChip® Operating Software (GCOS) (http://media.affymetrix.com/support/technical/whitepapers/sadd_whitepaper.pdf).

Data analysis

Data analyses were carried out with GeneSpring (Agilent Technologies, Santa Clara, CA, USA). All of the data from the VPA-treated groups were normalized to the median of the control groups, and the expression of each selected gene was calculated as a log ratio of the signal to the control value. To assess the differences between the control and VPA-treated groups, the Benjamini and Hochberg false-discovery rate (FDR) method was employed, and those with a p-value less than 0.05 were considered as significant. Network, function, and pathway analyses were performed using Ingenuity Pathway Analysis software (IPA; Ingenuity Systems, Redwood City, CA, USA).

RESULTS AND DISCUSSION

Behavioral tests for anxiety

The time spent in the open arms was significantly shorter in the males of P14SC than in those of the corresponding control, indicating enhanced anxiety by postnatal exposure to VPA (Fig. 2, left). There were, however, no significant changes in the behavior test of the females (Fig. 2, right). There were no effects of the VPA exposure on the number of entries into the open arms in both genders (data not shown). These results indicate that postnatal exposure to VPA caused enhanced anxiety specifically in males. This sexual dimorphism is a typical feature of autism and has been observed in the animal model for autism produced by prenatal exposure to VPA (Schneider *et al.*, 2008). We therefore analyzed the gene expression profile of the amygdala exposed to VPA only in males in the following experiments.

Gene expression microarray analysis

In the controls, gene expression profiles were almost identical among the varied VPA exposure conditions. The number of genes with expression levels different from those in the corresponding controls was larger in P14SC (53 probe sets for 49 genes) than in E12IP (32 probe sets for 30 genes), excluding expressed sequence tags (Fig. 3A). Functional classification of the genes also indicated the differences of gene expression between P12IP and P14SC (Fig. 3B). P14SC contained a wider variety of categories than E12IP; 'phosphatase' appeared only in E12IP, while 'cytokine', 'growth factor', 'lig-

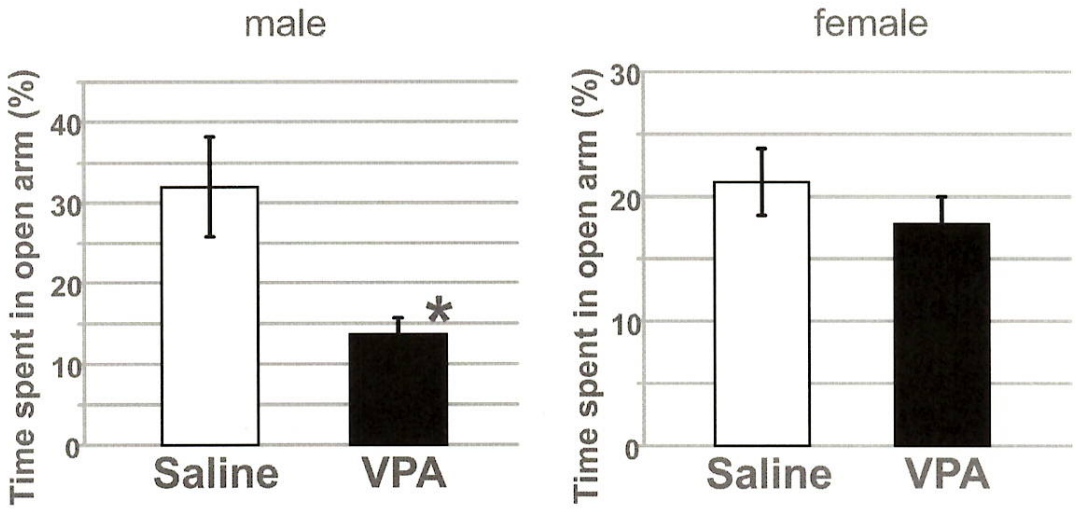

Fig. 2. The effects of postnatal exposure to VPA on anxiety-related behavior. 400 mg/kg VPA was administered to animals subcutaneously at P14. Anxiety-related behaviors were analyzed at 5w by EPM. Total open arm entries and time spent in open arm are quantified. The data of time spent in open arm were shown. An asterisk indicates a statistically significant difference from the control ($P < 0.05$, $N = 13$-15, Student's t test).

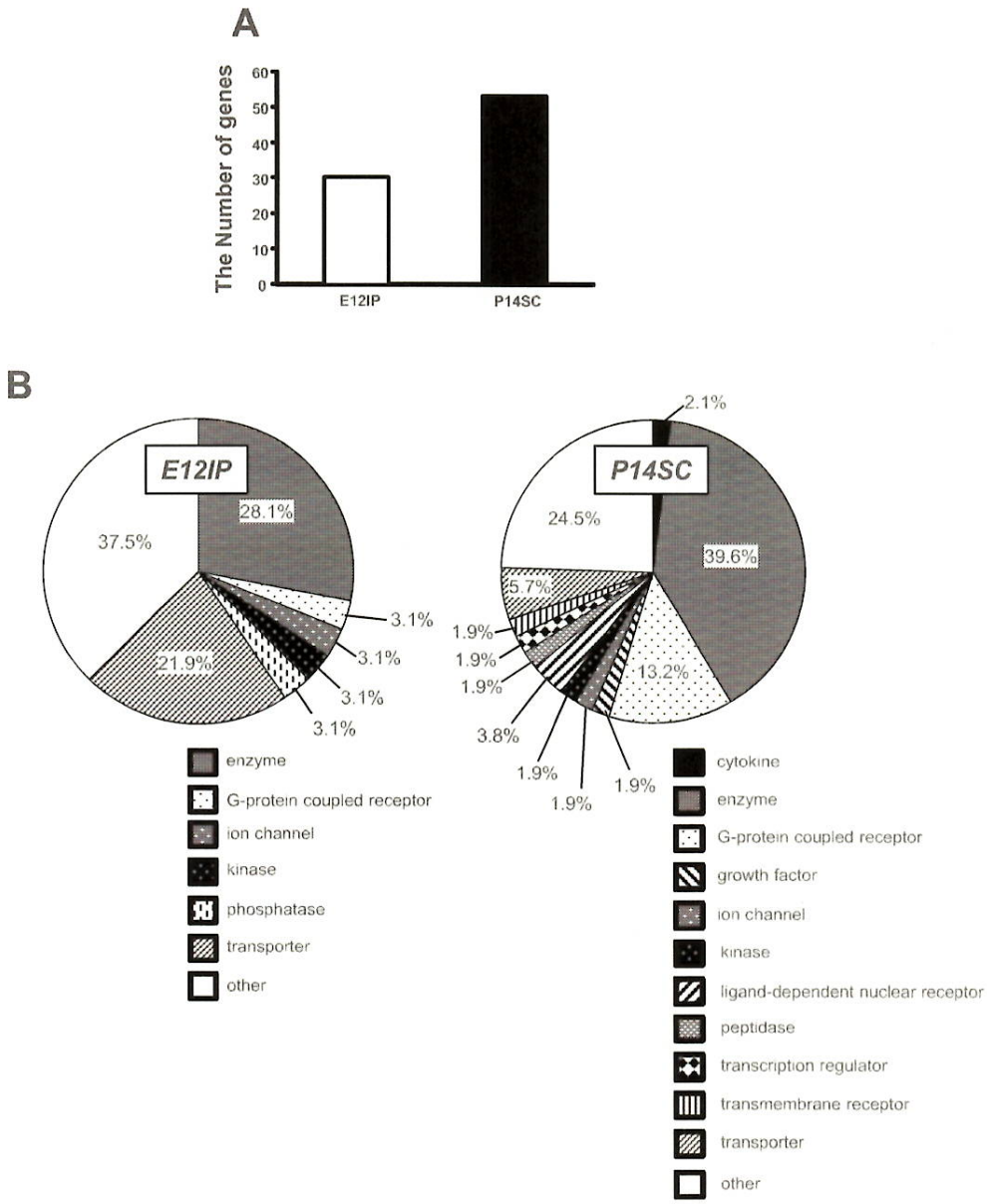

Fig. 3. Summary of the gene expression profiles of E12IP and P14SC rats (male). For both of E12IP and P14SC, total RNA of the amygdalae of 5w male rats (P33-37, N = 4) were analyzed with the microarray chip. Data were collected using Affymetrix GeneChip® Operating Software (GCOS) and analyzed using GeneSpring software. A. The numbers of significantly changed genes in E12IP and P14SC ($p < 0.05$, N = 4). B. Functional classification of the significantly changed genes by GeneSpring.

and-dependent nuclear receptor', 'peptidase', 'transcription regulator', and 'transmembrane receptor' appeared only in P14SC. As for categories common to E12IP and P14SC, their proportions were different from each other; e.g., 'transporters' accounted for 21.9% in E12IP but only 5.7% in P14SC.

Only two genes, Neu2 and Mt2a, exhibited the significant changes in the same direction in E12IP and P14SC

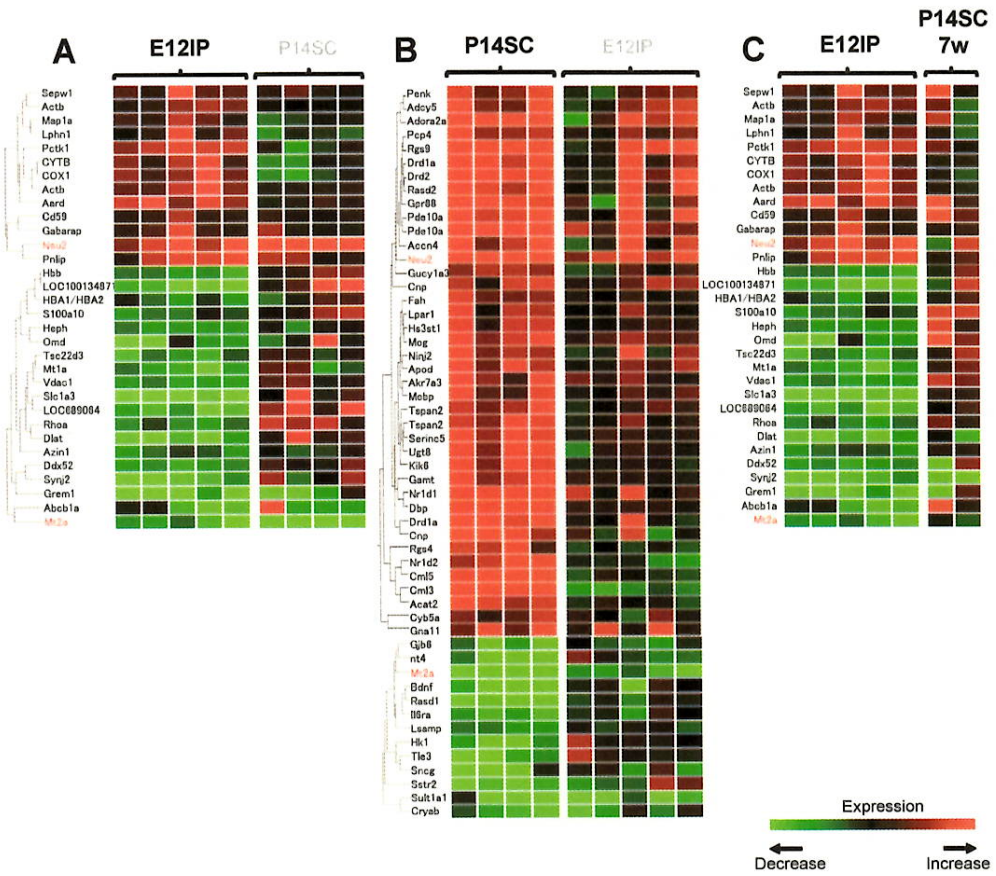

Fig. 4. Heat maps representing hierarchical clustering of the significantly changed genes of E12IP and P14SC. Each vertical column represents an individual sample, and each horizontal row represents a single gene. (N = 4 for P14SC and E12IP, N = 2 for P14SC7w) A. A heat map/hierarchical clustering of the significantly changed genes of E12IP with a heat map of the same genes of P14SC. Clustering was performed using the Benjamini and Hochberg FDR method. B. A heat map/hierarchical clustering of the significantly changed genes of P14SC with a heat map of the same genes of E12IP. C. A heat map of E12IP was compared with that of P14SC7w in which cRNA was extracted 7 w after VPA exposure at P14.

(red letters in Figs. 4A and B). The expression profile in E12IP was also different from that in P14SC7w (Fig. 4C), suggesting that the differences between E12IP and P14SC were not due to the varied length of time between the VPA exposure and the gene expression analysis. Precise gene lists for the heat maps of E12IP (Fig. 4A) and P14SC (Fig. 4B) are shown in Table 1 and Table 2, respectively. 'Behavior'-related genes were identified only in P14SC (Table 3). A larger number of genes were categorized as 'nervous system development and function', 'neurological disease' and 'psychological disorders' in P14SC than in E12IP.

Pathway analysis

The most significantly changed network (Fig. 5A [i]) was that linking 'cell death', 'cellular compromise', and 'neurological disease'. The hubs of this network were MYC, HTT, and CASP3, although the expression levels of these three genes remained unchanged. The second most significantly changed network was that linking 'cell death', 'neurological disease', and 'carbohydrate metabolism' (Fig. 5A [ii]). TNF, which plays an especially important role in cell death, was a highly interconnected node. In P14SC, three significant networks were identified (Fig. 5B [i]-[iii]). These networks are related to 'nucleic acid metabolism' (Fig. 5B [i]), 'cell signaling' (Fig. 5B

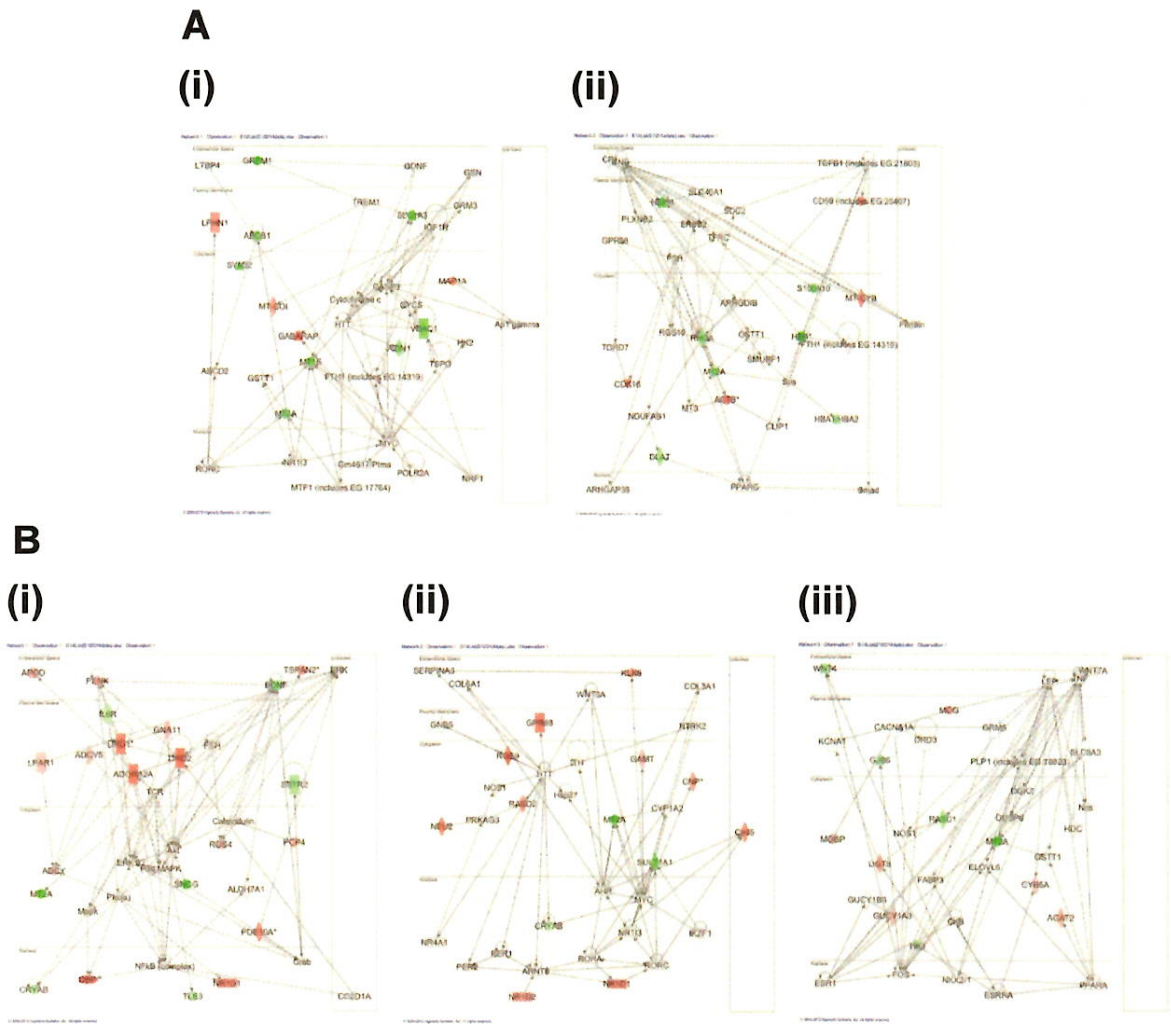

Fig. 5. IPA networks generated with significantly changed genes of E12IP and P14SC. A. The first (i) and second (ii) most significantly altered networks in E12IP. The most significantly changed network linked 'cell death', 'cellular compromise', and 'neurological disease'. The second most significantly changed network linked 'cell death', 'neurological disease', and 'carbohydrate metabolism'. B. The first (i), second (ii), and third (iii) most significantly changed networks in P14SC. These networks are related to 'nucleic acid metabolism' (i), 'cell signaling' (ii), and 'neurological disease' (iii).

[ii]), and 'neurological disease' (Fig. 5B [iii]). One notable aspect of these networks that was not observed in the E12IP networks is the alterations in the expression levels of nuclear genes such as DBP (transcription regulator), NR1D1 (nuclear receptor), and NR1D2 (nuclear receptor).

In conclusion, there are little similarities in the gene expression profiles between the two rat models for autism and regressive autism produced by pre- and post-natal exposures to VPA respectively. It is considered that that gene expression changes per se in the amygdala may be an important cause for impaired social behavior and enhanced anxiety, rather than expression changes of particular genes.

Table 1. The list of genes which changed significantly in E12IP

ID	Symbol	Entrez Gene name	Type(s)
Increase			
1389956_a_at	MT-COI	cytochrome c oxidase subunit I	enzyme
1367996_a_at	LPHN1	latrophilin 1	G-protein coupled receptor
1367882_at	MAP1A	microtubule-associated protein 1A	other
1388159_at	MT-CYB	cytochrome b	enzyme
1367929_at	CD59 (includes EG:25407)	CD59 molecule, complement regulatory protein	other
1398836_s_at	ACTB	actin, beta	other
1368127_at	NEU2	sialidase 2 (cytosolic sialidase)	enzyme
1398835_at	ACTB	actin, beta	other
1370326_at	CDK16	cyclin-dependent kinase 16	kinase
1370804_at	GABARAP	GABA(A) receptor-associated protein	transporter
1367593_at	SEPW1	selenoprotein W, 1	enzyme
1368554_at	PNLIP	pancreatic lipase	enzyme
1370459_at	C8orf85	chromosome 8 open reading frame 85	other
Decrease			
1387197_at	OMD	osteomodulin	other
1371245_a_at	HBB	hemoglobin, beta	transporter
1371130_at	SLC1A3	solute carrier family 1 (glial high affinity glutamate transporter), member 3	transporter
1368971_a_at	SYNJ2	synaptojanin 2	phosphatase
1371102_x_at	LOC100134871	beta globin minor gene	other
1369113_at	GREM1	gremlin 1	other
1371237_a_at	MT1E	metallothionein 1E	other
1368533_at	HEPH	hephaestin	transporter
1368588_at	DDX52	DEAD (Asp-Glu-Ala-Asp) box polypeptide 52	enzyme
1367771_at	Tsc22d3	TSC22 domain family, member 3	other
1386909_a_at	VDAC1	voltage-dependent anion channel 1	ion channel
1388271_at	MT2A	metallothionein 2A	other
1370464_at	ABCB1	ATP-binding cassette, sub-family B (MDR/TAP), member 1	transporter
1367553_x_at	HBB	hemoglobin, beta	transporter
1386890_at	S100A10	S100 calcium binding protein A10	other
1370575_a_at	AZIN1	antizyme inhibitor 1	enzyme
1370130_at	RHOA	ras homolog gene family, member A	enzyme
1388194_at	DLAT	dihydrolipoamide S-acetyltransferase	enzyme
1388608_x_at	HBA1/HBA2	hemoglobin, alpha 1	transporter

ID, symbol, entrez gene name, type of each gene were shown based on IPA software database.

Table 2. The list of genes which changed significantly in P14SC

ID	Symbol	Entrez Gene name	Type(s)
Increase			
1386904_a_at	CYB5A	cytochrome b5 type A (microsomal)	enzyme
1387897_at	CNP	2',3'-cyclic nucleotide 3' phosphodiesterase	enzyme
1370048_at	LPAR1	lysophosphatidic acid receptor 1	G-protein coupled receptor
1368092_at	FAH	fumarylacetoacetate hydrolase (fumarylacetoacetase)	enzyme
1368506_at	RGS4	regulator of G-protein signaling 4	other
1368298_at	ADCY5	adenylate cyclase 5	enzyme
1370834_at	HS3ST1	heparan sulfate (glucosamine) 3-O-sulfotransferase 1	enzyme
1368154_at	GUCY1A3	guanylate cyclase 1, soluble, alpha 3	enzyme
1368145_at	PCP4	Purkinje cell protein 4	other
1368253_at	GAMT	guanidinoacetate N-methyltransferase	enzyme
1387822_at	GNA11	guanine nucleotide binding protein (G protein), alpha 11 (Gq class)	enzyme
1368263_a_at	MOBP	myelin-associated oligodendrocyte basic protein	other
1367949_at	PENK	proenkephalin	other
1370206_at	ACCN4	amiloride-sensitive cation channel 4, pituitary	ion channel
1386979_at	SERINC5	serine incorporator 5	transporter
1368104_at	TSPAN2	tetraspanin 2	other
1372462_at	ACAT2	acetyl-CoA acetyltransferase 2	enzyme
1398257_at	MOG	myelin oligodendrocyte glycoprotein	other
1398258_at	APOD	apolipoprotein D	transporter
1368105_at	TSPAN2	tetraspanin 2	other
1368384_at	KLK6	kallikrein-related peptidase 6	peptidase
1370541_at	NR1D2	nuclear receptor subfamily 1, group D, member 2	ligand-dependent nuclear receptor
1370693_a_at	CNP	2',3'-cyclic nucleotide 3' phosphodiesterase	enzyme
1368121_at	AKR7A3	aldo-keto reductase family 7, member A3 (aflatoxin aldehyde reductase)	enzyme
1368438_at	PDE10A	phosphodiesterase 10A	enzyme
1368858_at	UGT8	UDP glycosyltransferase 8	enzyme
1370372_at	RASD2	RASD family, member 2	enzyme
1370816_at	NR1D1	nuclear receptor subfamily 1, group D, member 1	ligand-dependent nuclear receptor
1368478_at	DRD1	dopamine receptor D1	G-protein coupled receptor
1370669_a_at	PDE10A	phosphodiesterase 10A	enzyme
1387874_at	DBP	D site of albumin promoter (albumin D-box) binding protein	transcription regulator
1388176_at	Cml5	camello-like 5	enzyme
1368135_at	NINJ2	ninjurin 2	other
1368127_at	NEU2	sialidase 2 (cytosolic sialidase)	enzyme
1368479_at	DRD1	dopamine receptor D1	G-protein coupled receptor

Table 2. (Continued)

ID	Symbol	Entrez Gene name	Type(s)
Increase			
1387241_at	GPR88	G protein-coupled receptor 88	G-protein coupled receptor
1368708_a_at	DRD2	dopamine receptor D2	G-protein coupled receptor
1368300_at	ADPRA2A	adenosine A2a receptor	G-protein coupled receptor
1368500_a_at	RGS9	regulator of G-protein signaling 9	enzyme
1370991_at	Cml3/Gm4477	camello-like 3	enzyme
Decrease			
1370550_at	LSAMP	limbic system-associated membrane protein	other
1370026_at	CRYAB	crystallin, alpha B	other
1386987_at	IL6R	interleukin 6 receptor	transmembrane receptor
1368641_at	WNT4	wingless-like MMTV integration site family, member 4	cytokine
1387169_at	TLE3	transducin-like enhancer of split 3 (E(sp 1) homolog, Drosophila)	other
1368577_at	GJB6	gap junction protein, beta 6, 30kDa	transporter
1386929_at	HK1	hexokinase 1	kinase
1368782_at	SSTR2	somatostatin receptor 2	G-proein coupled receptor
1368677_at	BDNF	brain-derived neurotrophic factor	growth factor
1387908_at	RASD1	RAS, dexamethasone-induced 1	enzyme
1370019_at	SULT1A1	sulfotransferase family, cytosolic, 1A, phenol-preferring, member 1	enzyme
1398245_at	SNCG	synuclein, gamma (breast cancer-specific protein 1)	other
1388271_at	MT2A	metallothionein 2A	other

ID, symbol, entrez gene name, type of each gene were shown based on IPA software database.

Table 3. The list of genes which changed significantly in E12IP and P14SC were categorized to groups based on their functions using IPA software

E12IP			P14SC	
p-value	Molecules	Category	P14SC	p-value
		Behavior	RGS9,GJB6,RASD2,DBP,BDNF,PDE10A,IL6R,CNP,SNCG,DRD2,PCP4,DRD1,NR1D1,LPAR1,ADCY5,PENK,ADORA2A	2.16E-07-1.85E-02
1.02E-02-1.02E-02	RHOA	Cell Cycle	CRYAB,SSTR2,WNT4	4.65E-03-1.85E-02
6.33E-06-3.04E-02	ABCB1,CD59,MT2A,RHOA,ACTB,GREM1,VDAC1,MT1E	Cell Death	CRYAB,BDNF,IL6R,RGS4,UGT8,DRD2,HK1,LPAR1,SSTR2,ADCY5,MT2A,ADORA2A,MOG	3.03E-04-2.31E-02
2.56E-03-4.46E-02	CD59,HBB,MT2A,RHOA,SLC1A3,VDAC1	Cell Morphology	HK1,LPAR1,DRD1,MT2A,BDNF,IL6R,GNA11,KLK6,RGS4,SNCG,DRD2,ADORA2A	4.59E-04-2.31E-02
4.93E-02-4.93E-02	CD59,HBA1/HBA2,VDAC1	Cell Signaling	RGS9,LPAR1,SSTR2,DRD1,BDNF,ADCY5,PDE10A,IL6R,GNA11,RGS4,DRD2,ADORA2A	9.12E-05-2.07E-02
6.3E-05-2.54E-02	CD59,MT2A,RHOA,SLC1A3,GREM1,GABARAP,VDAC1,LPHN1,MT1E,S100A10	Cell-To-Cell Signaling and Interaction	RASD2,GUCY1A3,BDNF,GNA11,CNP,IL6R,RGS4,KLK6,SNCG,DRD2,PCP4,DRD1,ADCY5,MT2A,SULT1A1,PENK,ADORA2A,MOG,NINJ2	2.34E-07-2.31E-02
6.33E-06-4.27E-02	SYNJ2,CD59,MT2A,RHOA,HBA1/HBA2,VDAC1,LPHN1,MT1E	Cellular Assembly and Organization	RGS9,HK1,CRYAB,LPAR1,DRD1,MT2A,BDNF,GNA11,CNP,SNCG,DRD2,MOG	4.65E-03-2.31E-02
4.67E-04-4.46E-02	Tsc22d3,HBB,MT2A,RHOA,HBA1/HBA2,SLC1A3,	Cellular Development	NR1D1,DRD1,MT2A,BDNF,SERINC5,IL6R,RGS4,UGT8,DRD2	5.55E-04-2.31E-02
1.32E-04-4.27E-02	CD59,MT2A,RHOA,HBA1/HBA2,VDAC1,LPHN1,MT1E	Cellular Function and Maintenance	CRYAB,DRD1,BDNF,CNP	4.65E-03-2.31E-02
4.67E-04-2.07E-02	ABCB1,MT2A,RHOA,ACTB,GREM1,GABARAP,VDAC1,MT1E	Cellular Growth and Proliferation	GJB6,CRYAB,GUCY1A3,BDNF,IL6R,GNA11,KLK6,RGS4,SNCG,DRD2,RASD1,SSTR2,LPAR1,NR1D1,MT2A,PENK,WNT4,ADORA2A,MOG	3.03E-04-2.17E-02
2.56E-03-4.77E-02	CD59,RHOA,LPHN1,S100A10	Cellular Movement	GUCY1A3,BDNF,GNA11,CNP,IL6R,RGS4,KLK6,SNCG,DRD2,NR1D1,SSTR2,DRD1,LPAR1,PENK,ADORA2A,MOG	6.76E-05-1.85E-02
1.67E-05-2.54E-02	Tsc22d3,MT2A,RHOA,GREM1,VDAC1,MT1E	Connective Tissue Development and Function		
5.12E-03-4.27E-02	HBB,RHOA,PNLIP	Developmental Disorder	CRYAB,GJB6,SSTR2,DRD1,GUCY1A3,BDNF,IL6R,GNA11,WNT4,RGS4,DRD2	2.02E-05-2.31E-02
7.67E-03-7.67E-03	ABCB1	DNA Replication, Recombination, and Repair	GUCY1A3,BDNF,RGS4,DRD2,ADORA2A	1.28E-02-1.28E-02
2.56E-03-4.27E-02	ABCB1	Drug Metabolism	DRD1,BDNF,SULT1A1,GNA11,RGS4,SNCG,DRD2,ADORA2A	2.12E-05-1.85E-02
2.56E-03-4.77E-02	HBB,RHOA,GREM1	Embryonic Development	GJB6,LPAR1,BDNF,WNT4,KLK6,DRD2	1.17E-03-1.85E-02
2.56E-03-2.56E-03	ABCB1	Endocrine System Development and Function	BDNF,SULT1A1,GNA11,WNT4,ADORA2A	2.1E-04-2.31E-02
2.25E-02-2.25E-02	MT1E,S100A10	Endocrine System Disorders	ACAT2,SSTR2,DRD1,IL6R,DRD2	2.02E-05-2.31E-02
4.52E-02-4.52E-02	RHOA	Gene Expression	DBP,BDNF,IL6R,RGS4,KLK6,NR1D2,DRD2,RASD1,NR1D1,DRD1,LPAR1,TLE3,WNT4,ADORA2A,MOG	1.38E-02-1.39E-02

Table 3. (Continued)

E12IP			P14SC	
p-value	Molecules	Category	P14SC	p-value
1.29E-03-4.27E-02	ABCB1,HBB,MT2A,ACTB,PNLIP,MT1E	Genetic Disorder	ACCN4,RGS9,CRYAB,GJB6,RASD2,ACAT2,BDNF,GNA11,KLK6,NR1D2,DRD1,ADCY5,MT2A,WNT4,LSAMP,MOG,GUCY1A3,DBP,PDE10A,CNP,IL6R,TSPAN2,RGS4,NEU2,SNCG,DRD2,GPR88,FAH,PCP4,LPAR1,NR1D1,MOBP,SSTR2,SULT1A1,PENK,TLE3,CYB5A,ADORA2A,APOD	4.1E-09-2.31E-02
2.56E-03-4.27E-02	ABCB1,RHOA,MT1E	Inflammatory Disease	CRYAB,BDNF,IL6R,DRD2,MOG	4.65E-03-2.31E-02
2.56E-03-4.27E-02	CD59,RHOA,MT1E,S100A10	Inflammatory Response	GNA11,IL6R,PENK,CNP,ADORA2A,MOG	9.29E-03-2.31E-02
2.56E-03-4.4E-02	SYNJ2,ABCB1,MT2A,DLAT,RHOA,MT1E,PNLIP,S100A10	Lipid Metabolism	ACAT2,DBP,BDNF,SERINC5,GNA11,RGS4,UGT8,DRD2,LPAR1,DRD1,SSTR2,SULT1A1,WNT4,ADORA2A,MOG,APOD	2.1E-04-2.31E-02
6.33E-06-4.93E-02	ABCB1,CD59,HBA1/HBA2,CDK16,SLC1A3,HEPH,LPHN1,HBB,MT-CYB,MT2A,RHOA,GABARAP,VDAC1,MT1E,PNLIP,S100A10	Molecular Transport	ACAT2,GUCY1A3,BDNF,PDE10A,GNA11,IL6R,RGS4,UGT8,SNCG,DRD2,HK1,LPAR1,SSTR2,DRD1,MT2A,ADCY5,WNT4,ADORA2A,APOD	1.11E-05-2.31E-02
3.99E-03-4.27E-02	MT2A,RHOA,HBA1/HBA2,SLC1A3,GABARAP,VDAC1,LPHN1,MT1E	Nervous System Development and Function	GJB6,RASD2,GUCY1A3,DBP,BDNF,SERINC5,CNP,GNA11,RGS4,UGT8,SNCG,DRD2,PCP4,DRD1,NR1D1,LPAR1,ADCY5,MT2A,PENK,ADORA2A,MOG,NINJ2	1.59E-05-2.31E-02
3.79E-05-3.78E-02	MT2A,ACTB,SLC1A3,MT1E,S100A10	Neurological Disease	RGS9,CRYAB,RASD2,GJB6,BDNF,GNA11,DRD1,MT2A,ADCY5,LSAMP,MOG,GUCY1A3,DBP,PDE10A,CNP,IL6R,RGS4,SNCG,DRD2,GPR88,PCP4,LPAR1,MOBP,SSTR2,NR1D1,PENK,ADORA2A,APOD	1.43E-09-2.31E-02
2.64E-02-2.64E-02	MT2A,MT1E	Psychological Disorders	CRYAB,BDNF,PDE10A,CNP,RGS4,DRD2,PCP4,MOBP,DRD1,SSTR2,MT2A,LSAMP,ADORA2A,MOG,APOD	1.57E-04-2.01E-02
6.33E-06-4.4E-02	ABCB1,AZIN1,HBA1/HBA2,SLC1A3,SYNJ2,HBB,MT2A,RHOA,DLAT,VDAC1,PNLIP,MT1E,S100A10	Small Molecule Biochemistry	RGS9,ACAT2,BDNF,SERINC5,GNA11,HK1,DRD1,MT2A,ADCY5,WNT4,MOG,DBP,GUCY1A3,PDE10A,IL6R,RGS4,UGT8,SNCG,DRD2,SSTR2,LPAR1,GAMT,SULT1A1,CYB5A,ADORA2A,APOD	1.11E-05-2.31E-02
2.56E-03-2.79E-02	CD59,Tsc22d3,HBB,RHOA,SLC1A3,GREM1	Tissue Development	GJB6,CRYAB,GUCY1A3,BDNF,GNA11,CNP,IL6R,KLK6,RGS4,DRD2,GAMT,DRD1,LPAR1,TLE3,WNT4,ADORA2A,MOG,NINJ2	4.59E-04-2.31E-02
3.43E-04-2.79E-02	CD59,HBB,MT2A,RHOA,SLC1A3,GREM1,MT1E,S100A10	Tissue Morphology	CRYAB,ACAT2,GUCY1A3,BDNF,IL6R,DRD2,GAMT,DRD1,SSTR2,LPAR1,WNT4,ADORA2A,MOG	8E-04-2.31E-02

Behavior'-related genes were identified only in P14SC. Additionally a larger number of genes were categorized to 'nervous system development and function', 'neurological disease', and 'psychological disorders' in P14SC than in E12IP.

ACKNOWLEDGMENT

This work was supported by Grants-in-Aid from the Food Safety Commission of Japan (No. 1003).

REFERENCES

Blackford, J.U. and Pine, D.S. (2012): Neural substrates of childhood anxiety disorders: a review of neuroimaging findings. Child Adolesc. Psychiatr. Clin. N. Am., **21**, 501-525.

Etkin, A. and Wager, T.D. (2007): Functional neuroimaging of anxiety: a meta-analysis of emotional processing in PTSD, social anxiety disorder, and specific phobia. Am. J. Psychiatry., **164**, 1476-1488.

Markram, K., Rinaldi, T., Mendola, D.L., Sandi, C. and Markram, H. (2008): Abnormal fear conditioning and amygdala processing in an animal model of autism. Neuropsychopharmacology, **33**, 901-912.

Neuhaus, E., Beauchaine, T.P. and Bernier, R. (2010): Neurobiological correlates of social functioning in autism. Clin. Psychol. Rev., **30**, 733-748.

Schneider, T. and Przewtocki, R. (2005): Behavioral alterations in rats prenatally exposed to valproic acid: Animal model of autism. Neuropsychopharmacology, **30**, 80-89.

Schneider, T., Ziolkowska, T., Gieryk, T., Tyminska, T. and Przewlocki, R. (2007): Prenatal exposure to valproic acid disturbs the enkephalinergic system functioning, basal hedonic tone, and emotional responses in an animal model of autism. Psychopharmacology, **193**, 547-555.

Schneider, T., Roman, A., Basta-Kaim, A., Kubera, M., Budziszewska, B., Schneider, K. and Przewtochi, R. (2008): Gender-specific behavioral and immunological alterations in an animal model of autism induced by prenatal exposure to valproic acid. Psychoneuroendocrinology, **33**, 728-740.

Wagner, G.C., Reuhl, K.R., Cheh, M., McRae, P. and Halladay, A.K. (2006): A new neurobehavioral model of autism in mice: Pre- and postnatal exposure to sodium valproate. J Autism Dev. Disord., **36**, 779-793.

Yochum, C.L., Dowling, P., Reuhl, K.R., Wagner, G.C. and Ming, X. (2008): VPA-induced apoptosis and behavioral deficits in neonatal mice. Brain Res., **1203**, 126-132.

Yochum, C.L., Bhattacharya, P., Patti, L., Mirochnitchenko, L. and Wagner, G.C. (2010): Animal model of autism using GSTM1 knockout mice and early post-natal sodium valproate treatment. Behav. Brain Res., **210**, 202-210.

Niflumic Acid Activates Additional Currents of the Human Glial L-Glutamate Transporter EAAT1 in a Substrate-Dependent Manner

Kanako Takahashi,[a] Reiko Ishii-Nozawa,[b] Koichi Takeuchi,[b] Ken Nakazawa,[a] Yuko Sekino,[a] and Kaoru Sato*,[a]

[a] *Laboratory of Neuropharmacology, Division of Pharmacology, National Institute of Health Sciences; 1–18–1 Kamiyoga, Setagaya, Tokyo 158–8501, Japan: and* [b] *Department of Clinical Pharmacology, Meiji Pharmaceutical University; 2–522–1 Noshio, Kiyose, Tokyo 204–8588, Japan.*
Received September 6, 2013; accepted September 29, 2013

The astrocytic L-glutamate (L-Glu) transporter EAAT1 participates in the removal of L-Glu from the synaptic cleft and maintenance of non-toxic concentrations in the extracellular fluid. We have shown that niflumic acid (NFA), a non-steroidal anti-inflammatory drug (NSAIDs), alters L-Glu-induced EAAT1 currents in a voltage-dependent manner using the two-electrode voltage clamp technique in *Xenopus* oocytes expressing EAAT1. In this study, we characterised the effects of NFA on each type of ion-flux through EAAT1. NFA modulated currents induced by both L-Glu and L-aspartate (L-Asp) in a voltage-dependent manner. Ion-substitution experiments revealed that the activation of additional H^+ conductance was involved in the modulation of currents induced by L-Asp and L-Glu, but Cl^- was involved only with the L-Asp currents. NFA activated additional currents of EAAT1 in a substrate-dependent manner.

Key words astrocytic L-glutamate transporter; niflumic acid; additional conductance; EAAT1; voltage-dependent manner

Neuronal and astrocytic L-glutamate (L-Glu) transporters (EAATs) are the only significant machinery for the removal of L-Glu from the synaptic cleft and maintenance of non-toxic concentrations in the extracellular fluid.[1] Along with controlling extracellular L-Glu concentrations, EAATs also play a role in the regulation of functional crosstalk between neurons and glial cells by modulating the ion flux. L-Glu is co-transported into a cell with 3 Na^+ and 1 H^+ by EAATs, followed by the counter-transport of 1 K^+ [2]. L-Glu and Na^+ binding to EAATs activates a non-stoichiometrically-coupled (uncoupled) Cl^- conductance.[3] The Na^+ influx triggers functional metabolic crosstalk between neurons and astrocytes,[4] and the uncoupled Cl^- conductance dampens neuronal excitability.[5,6]

Niflumic acid [2-((3-(trifluoromethyl)phenyl)amino)-3-pyridinecarboxylic acid, NFA], a member of a class of non-steroidal anti-inflammatory drugs (NSAIDs), modulates the gating of Cl^- channels,[7,8] K^+ channels,[9–14] nicotinic acetylcholine channels,[15] and transient receptor potential channels.[16] NFA also enhances the substrate-gated currents of EAAT4, an L-Glu transporter expressed primarily in Purkinje neurons,[17] by activating additional uncoupled H^+ and Cl^- conductances.[18] We recently discovered that NFA modulates the current mediated through EAAT1, an astrocytic L-Glu transporter,[19,20] in a voltage-dependent manner.[21] In this study, we characterised the effects of NFA on L-Glu and L-aspartate (L-Asp) currents, focusing on each ion-flux. We report here that the activation of additional H^+ conductance was involved in the modulation by NFA of both L-Glu currents and L-Asp currents, whereas Cl^- was involved only in the modulation of L-Asp currents.

MATERIALS AND METHODS

Expression of EAAT1 in *Xenopus* Oocytes All of the animals were treated in accordance with the guidelines for the Care and Use of Laboratory Animals of the Animal Research Committee of the National Institute of Health Sciences, Japan. A pcDNA3.1 plasmid containing the cDNA of the human glutamate transporter EAAT1 was obtained from Dr. Keiko Shimamoto (Suntory Institute for Bioorganic Research, Osaka, Japan). The plasmids containing the EAAT1 cDNA were linearized at a *Not*I (Toyobo, Osaka, Japan) site, and capped RNA was transcribed from the linearized cDNA construct with a bacteriophage T7 RNA polymerase (mMESSAGE mMACHINE; Ambion, Austin, TX, U.S.A.). Oocytes were collected from anaesthetised *Xenopus laevis*. The isolated oocytes were then treated with collagenase (2 mg mL^{-1}, type 1, Sigma, St. Louis, MO, U.S.A.), and capped mRNA was injected into either defolliculated stage V or VI oocytes. The oocytes were incubated for 2–7 d at 18°C in ND96 solution containing 96 mM NaCl, 2 mM KCl, 1.8 mM $CaCl_2$, 1 mM $MgCl_2$, and 5 mM *N*-(2-hydroxyethyl)piperazine-*N'*-(2-ethanesulfonic acid) (HEPES) (pH 7.5) supplemented with 0.01% gentamycin.

Electrophysiology Two-electrode voltage clamp recordings from EAAT1-expressing oocytes were performed at room temperature (25–27°C) using glass microelectrodes filled with 3 M KCl solution (resistance=1–4 MΩ) and an Ag/AgCl pellet bath ground (EP2; World Precision Instruments, Sarasota, FL, U.S.A.). A bath-clamp amplifier (OC-725C; Warner Instruments, Hamden, CT, U.S.A.) was used with a Digidata 1320A interface (Axon Instruments, Foster City, CA, U.S.A.). The pClamp suite of programs (ver. 8.2; Axon Instruments) and the Clampfit data acquisition software were used to control stimulation parameters, and to acquire and analyse data. An Ag/AgCl pellets were used to avoid voltage errors associated with buffer changes. Oocytes were continuously superfused with ND96 solution. To adjust the extracellular H^+ to various concentrations, the HEPES was replaced by either 2-(*N*-morpholino)ethanesulfonic acid (MES) (pH 5.5, 6.5) or [(2-hydroxy-1,1-bis(hydroxymethyl)ethyl)amino]-1-propanesulfonic acid (TAPS) (pH 8.5). For Na^+ substitution experiments, Na^+ was replaced by equimolar choline ions. For

The authors declare no conflict of interest.

* To whom correspondence should be addressed. e-mail: kasato@nihs.go.jp

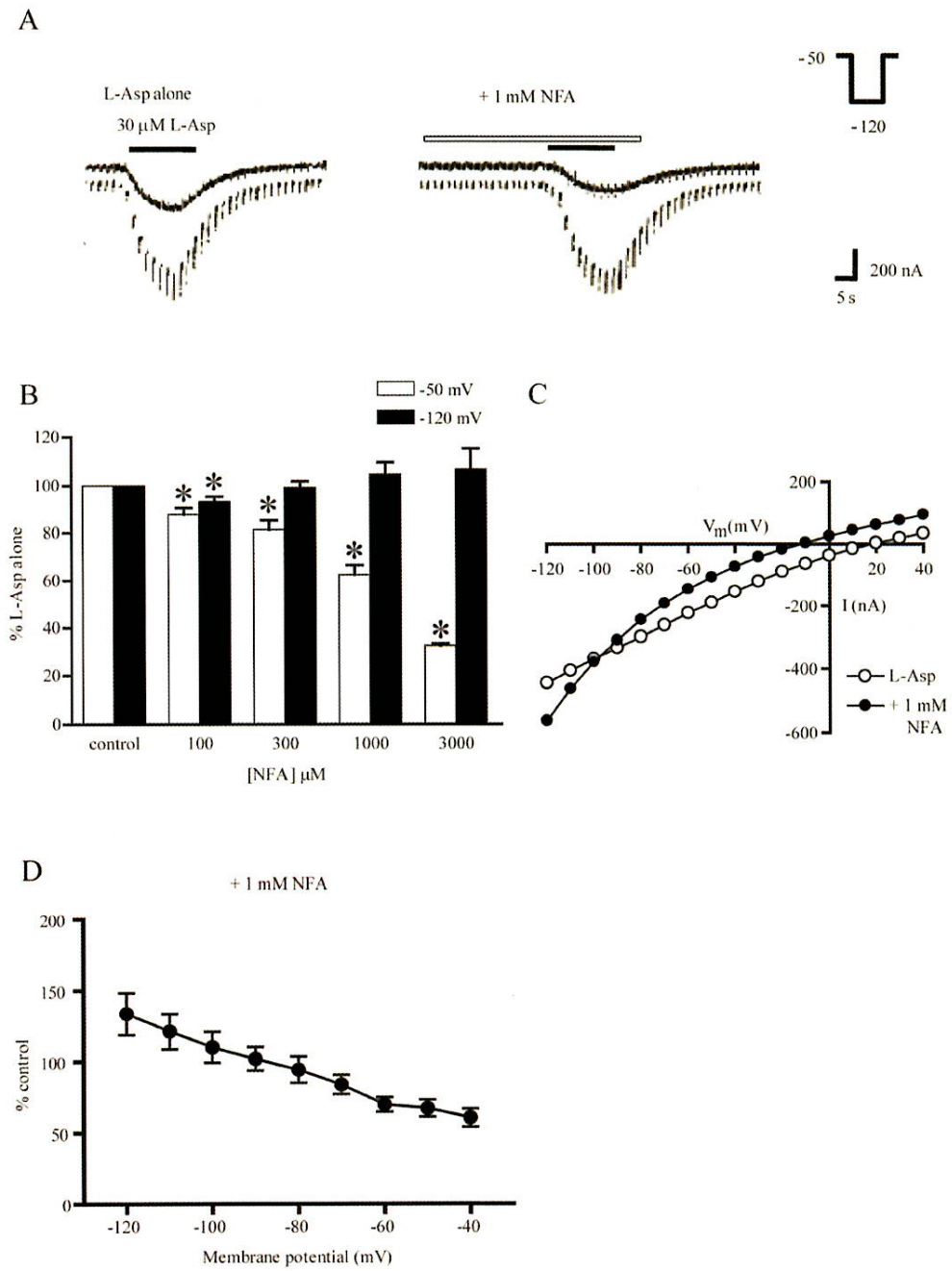

Fig. 1. Niflumic Acid (NFA) Modulated L-Asp-Induced Currents in *Xenopus* Oocytes Expressing EAAT1 in a Voltage-Dependent Manner

A: The traces of L-Asp (30 μM)-induced inward currents in either the absence or presence of NFA (1 mM) at −50 mV (bold line) and −120 mV (thin line). The oocytes were held at −50 mV and hyperpolarised to −120 mV for 400 ms every 2 s. B: Concentration–response relationships of the effects of NFA on L-Asp currents at −50 mV and −120 mV. The effects of NFA on the peak amplitude of the L-Asp current were examined by comparing the current in the presence of NFA to that recorded just prior to the drug treatment (control response) at each concentration. Data are analysed by paired *t*-test. Graph shows the summary of the results. Each column shows the averaged data normalized to the control (4–5 oocytes for each) at each concentration. At −50 mV, NFA inhibited the peak amplitudes of the L-Asp currents in a concentration-dependent manner, whereas NFA only slightly increased the peak amplitude of the L-Asp-induced currents at −120 mV. *$p<0.05$ *vs.* control. C: Representative current–voltage relationships for L-Asp (30 μM) in either the absence or presence of NFA (1 mM). The current–voltage relationships were obtained with a holding potential of −50 mV and implementation of 400-ms voltage jumps in 10 mV increments over the range from −120 mV to +40 mV. For the control, the current values at steady state were subtracted from those measured in the presence of L-Asp. For the NFA-treated group, the current values in the presence of NFA alone were subtracted from those in the presence of both NFA and L-Asp. NFA treatment produced a leftward shift of E_{rev} (from 18.4±5.4 to −2.7±4.1 mV; $n=10$, $p<0.05$, paired *t*-test). D: The relationship between the effects and the holding potential. The current in the presence of NFA was normalized to that obtained just before the application of NFA. The effects of NFA was voltage-dependent ($n=10$).

the Cl^- substitution experiments, Cl^- was replaced by equimolar gluconate ions. Oocytes were bathed in an experimental chamber (0.5 mL) filled with ND96 solution and voltage-clamped at −50 mV. A 400 ms hyperpolarising voltage step to −120 mV was applied every 2 s to confirm clamp conditions and observe the voltage dependence of current responses. As

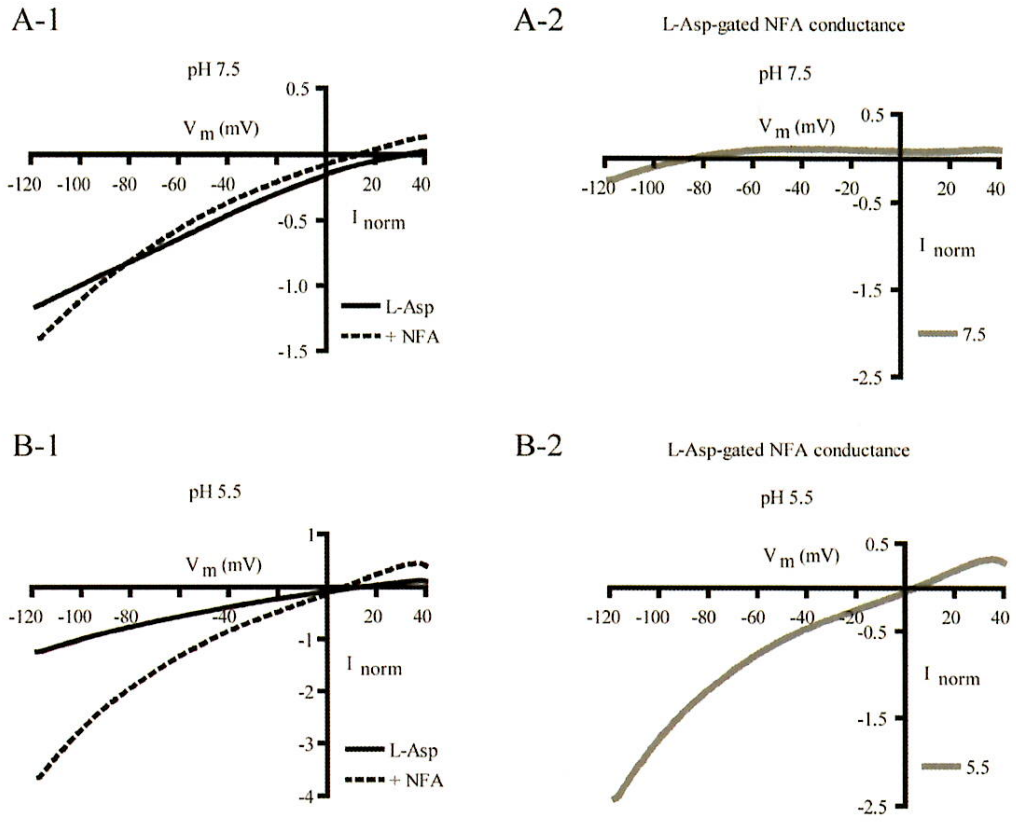

Fig. 2. Influence of Extracellular pH on L-Asp Currents in Either the Absence or Presence of NFA

The current–voltage relationships were determined using a holding potential of −50 mV and implementing an 800 ms ramp pulse over the range from +40 mV to −120 mV. The current–voltage relationships for the L-Asp-gated NFA-induced conductance were obtained by subtracting the control L-Asp currents from the L-Asp currents in the presence of NFA. The currents are normalised to the amplitude of the L-Asp currents generated at −100 mV. A-1 and B-1: Average current–voltage relationships for L-Asp (30 μM) in either the absence (solid line) or presence (dotted line) of NFA (300 μM) at pH 7.5 (A-1) and pH 5.5 (B-1). A-2 and B-2: Average current–voltage relationships for the L-Asp-gated NFA-induced conductance at pH 7.5 (A-2) and pH 5.5 (B-2). The average shift of the sub-E_{rev} was −45.1±4.0 mV per pH unit, which is consistent with that reported for H^+-selective channels. Each point represents the mean value from 5 oocytes.

a substrate, 30 μM of either L-Glu or L-Asp (half of the EC_{50}) was applied to the oocytes by superfusion at 0.2 mL·s^{-1} of constant flow rate for 15 s with regular 30 s intervals. NFA was applied from 30 s before to 5 s after the end of the application of substrate. The current–voltage relationships for substrate transport were determined by subtracting the steady-state currents obtained with a holding potential of −50 mV either implementing 400 ms voltage jumps in 10 mV increments from −120 to +60 mV or implementing an 800 ms ramp pulse from −120 to +40 mV in the absence of substrate from the corresponding currents in the presence of substrate. The currents are normalised to the amplitude of the L-Asp or L-Glu currents generated at −100 mV (Figs. 2–8).

Preparation of the Compounds All chemicals were purchased from Wako (Tokyo, Japan) unless otherwise stated. NFA, TAPS, and MES were purchased from Sigma (St. Louis, MO, U.S.A.). L-Asp and L-Glu stock solutions (20 mM) were made in purified water (Millipore, Billerica, MA, U.S.A.). The NFA stock solution (300 mM) was made in dimethyl sulfoxide (DMSO) and dissolved in ND96 solution immediately prior to each experiment. The pH of every solution was adjusted to 7.5, and the final concentrations of the solvents were less than 1%.

Statistical Analysis All of the data are presented as the mean±S.E.M. p Values were obtained by statistical analysis, as noted in the figure legends.

RESULTS

Effects of NFA on L-Asp-Induced Currents in *Xenopus* Oocytes Expressing EAAT1 We first examined the effects of NFA on the L-Asp-induced currents in *Xenopus* oocytes expressing EAAT1. The left trace in Fig. 1A represents the inward control current produced by L-Asp (30 μM) voltage clamped at −50 mV with 400 ms hyperpolarising voltage steps to −120 mV every 2 s. At −50 mV, NFA (300 μM–3 mM) inhibited the peak amplitude of the L-Asp-induced currents in a concentration-dependent manner, whereas at 120 mV, NFA only slightly increased the peak amplitude of the L-Asp-induced currents (Figs. 1A, B). Figure 1C shows the representative current–voltage relationships for L-Asp (30 μM)-induced currents in either the presence or absence of 1 mM NFA. In the absence of NFA, the L-Asp current was linear in a voltage-dependent manner, with the reversal potential (E_{rev}) at 18.4±5.4 mV. NFA treatment resulted in a leftward shift of the E_{rev} of the L-Asp currents (from 18.4±5.4 to −2.7±4.1 mV; n=10, p<0.05, paired t-test). The current–voltage curve recorded in the presence of NFA crossed the control curve at

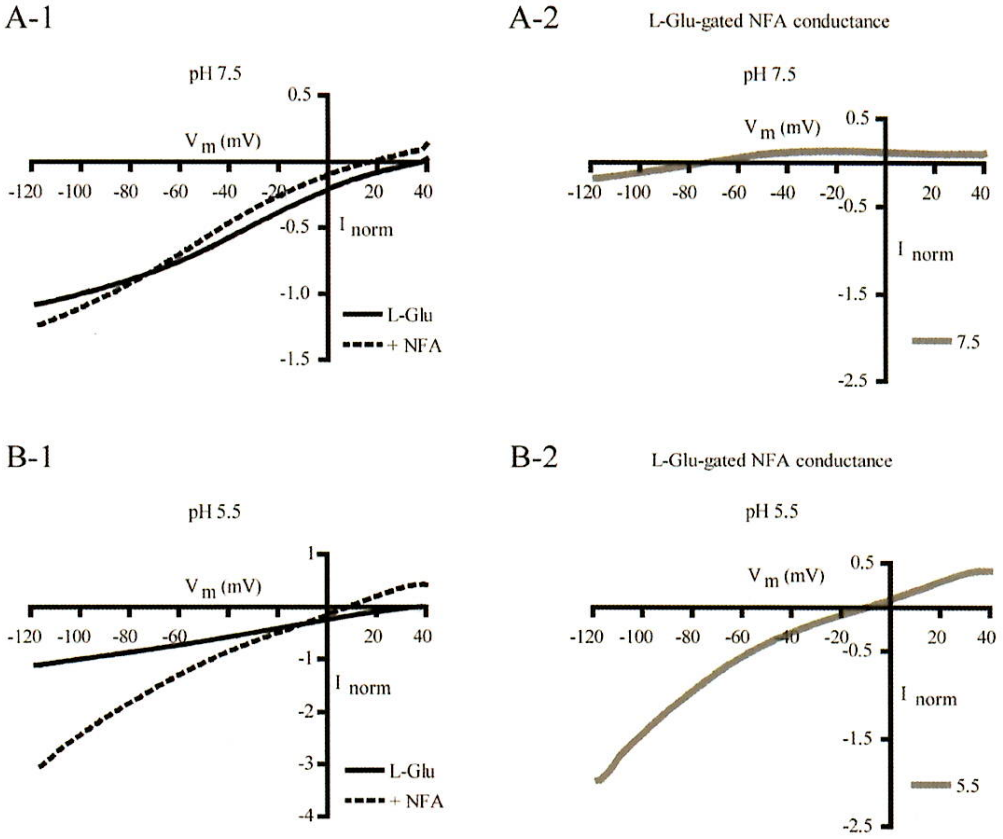

Fig. 3. Influence of Extracellular pH on L-Glu Currents in Either the Absence or Presence of NFA

A-1 and B-1: Average current–voltage relationships for L-Glu (30 μM) in either the absence (solid line) or presence (dotted line) of NFA (300 μM) at pH 7.5 (A-1) and pH 5.5 (B-1). A-2 and B-2: Average current–voltage relationships for the L-Glu-gated NFA-induced conductance at pH 7.5 (A-2) and pH 5.5 (B-2). The average shift of the sub-E_{rev} was -36.6 ± 4.6 mV per pH unit, which is consistent with that reported for H^+-selective channels. Each point represents the mean value from 5 oocytes.

-96.5 mV (cross-over potential), indicating that NFA inhibited the L-Asp currents at potentials more positive than -96.5 mV and increased the currents at potentials more negative than -96.5 mV. The influence of NFA on the peak current amplitude was voltage-dependent (Fig. 1D). This voltage-dependent effect of NFA has also been observed with L-Glu current in our previous study.[21]

Involvement of Additional H^+ Conductance We examined whether any additional H^+ conductance is involved in these voltage-dependent effect of NFA. The effects of NFA were examined when the extracellular pH was 7.5 and 5.5. Figures 2A-1 and B-1 show the average current–voltage relationships for the L-Asp current (30 μM) in either the absence (solid line) or presence (dotted line) of NFA (300 μM) at pH 7.5 (Fig. 2A-1) and pH 5.5 (Fig. 2B-1). At pH 7.5, the curve of the L-Asp current in the presence of NFA crossed the control curve at -84 mV, whereas the crossover potential was at $+4$ mV at pH 5.5. The L-Asp-gated NFA-induced conductance was obtained by subtracting the L-Asp current from the L-Asp current in the presence of NFA (Figs. 2A-2, B-2). As the extracellular H^+ concentration increased, the E_{rev} of the L-Asp-gated NFA-induced conductance (sub-E_{rev}) shifted toward the more positive membrane potential. The average shift of the sub-E_{rev} gated by L-Asp was -45.1 ± 4.0 mV per pH unit (n=5), which is consistent with previous reports for H^+-selective channels,[22,23] suggesting that NFA promotes additional H^+ conductance. Regarding L-Glu currents (Fig. 3), as the extracellular H^+ concentrations increased, the crossover potential shifted toward the more positive potential (Figs. 3A-1, B-1), and the sub-E_{rev} also shifted toward a more positive membrane potential (Figs. 3A-2, B-2). The average shift of the sub-E_{rev} gated by L-Glu changed -36.6 ± 4.6 mV per pH unit (n=5), suggesting that NFA promotes additional H^+ conductance in this case as well. There were no significant differences between the average shifts of the sub-E_{rev} per pH unit gated by L-Asp and L-Glu (Student's t-test, p=0.2).

Involvement of Additional Na^+ Conductance We examined if the additional Na^+ conductance is involved in these voltage-dependent effect of NFA. The current–voltage relationships for the L-Asp current in either the absence or presence of NFA were examined under various extracellular [Na^+] by choline substitution. Figures 4A-1 and B-1 show the average current–voltage relationships for L-Asp in either the absence (solid line) or presence (dotted line) of NFA (300 μM) at normal [Na^+] (96 mM) (Fig. 4A-1) and low [Na^+] (24 mM) (Fig. 4B-1). Decreasing the extracellular [Na^+] resulted in a loss of crossover between -120 mV and $+40$ mV, indicating that low extracellular [Na^+] results in a loss of the voltage-dependent modulation of L-Asp currents by NFA. The L-Asp-gated NFA-induced conductance-voltage relationships displayed inward rectification with the sub-E_{rev} at -58 mV (Fig. 4A-2) at normal [Na^+], whereas no significant subtracted currents

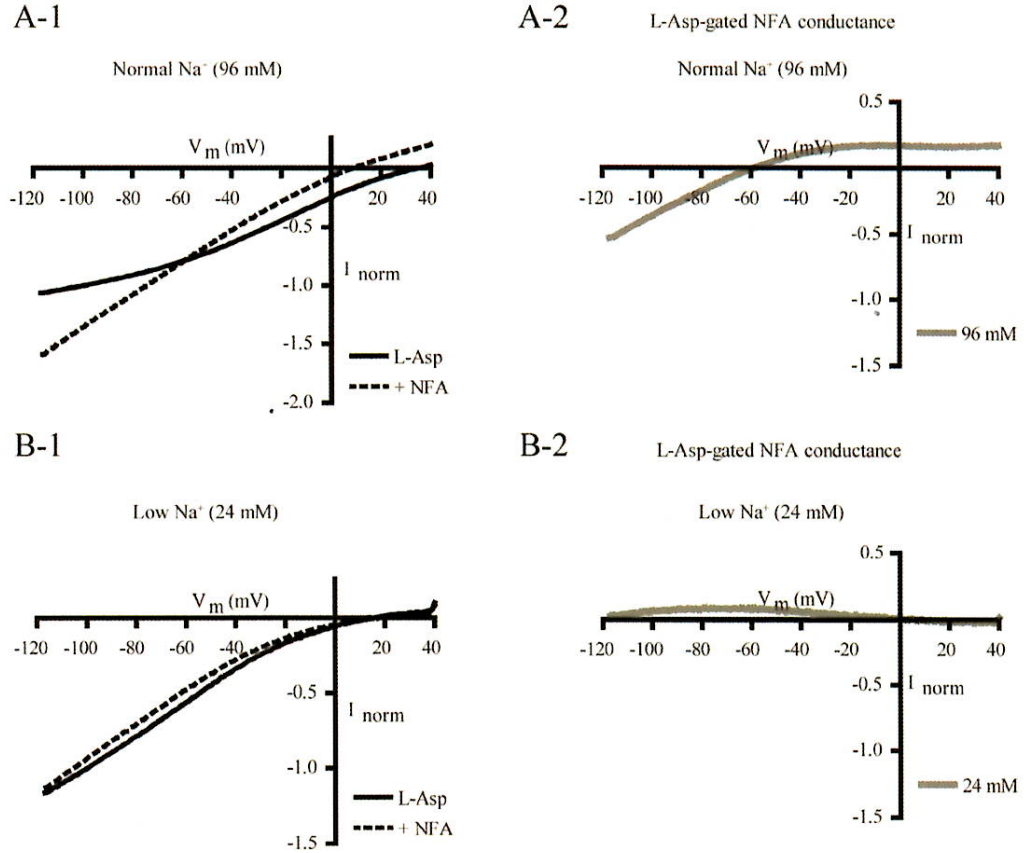

Fig. 4. Influence of Extracellular [Na^+] on L-Asp-Gated NFA-Induced Conductance and the L-Asp Currents in Either the Absence or Presence of NFA

The current–voltage relationships for the L-Asp current in either the absence or presence of NFA were examined under various extracellular [Na^+] by choline substitution. A-1 and B-1: Average current–voltage relationships for L-Asp (30 μM) in either the absence (solid line) or presence (dotted line) of NFA (300 μM) at normal [Na^+] (96 mM) (A-1) and low [Na^+] (24 mM) (B-1). A-2 and B-2: Average current–voltage relationships for the L-Asp-gated NFA-induced conductance at normal [Na^+] (96 mM) (A-2) and low [Na^+] (24 mM) (B-2). The average shift of the sub-E_{rev} gated by L-Asp was -1.1 ± 12.4 mV (n=3) per 10-fold change in [Na^+]. Each point represents the mean from 3 oocytes.

were observed at low [Na^+], suggesting that the modulation of L-Asp currents by NFA depends on the extracellular Na^+ concentration. Comparing the sub-E_{rev} at normal [Na^+] (96 mM) with that at middle-low [Na^+] (48 mM), the average shift of the sub-E_{rev} gated by L-Asp was -1.1 ± 12.4 mV (n=3) per 10-fold change in [Na^+]. In the case of L-Glu, decreasing the extracellular [Na^+] also resulted in a loss of crossover between -120 mV and $+40$ mV (Figs. 5A-1, B-1). The sub-E_{rev} gated by L-Glu was -68 mV at normal [Na^+], whereas no significant subtracted currents were observed at low [Na^+] (Figs. 5A-2, B-2), suggesting that the voltage-dependent modulation of L-Glu currents by NFA depends on the extracellular Na^+ concentration. Comparing the sub-E_{rev} at normal [Na^+] with that at middle-low [Na^+], the average shift of the sub-E_{rev} gated by L-Glu was 7.8 ± 2.2 mV (n=3) per 10-fold change in [Na^+]. This value was not significantly different from that for L-Asp (Student's t-test, p=0.5).

Involvement of Additional Cl^- Conductance Finally, we examined the contribution of additional Cl^- conductance. The current–voltage relationships for the L-Asp current in either the absence or presence of NFA were examined under various extracellular [Cl^-] by gluconate substitution. Figures 6A-1 and B-1 show the average current–voltage relationships for L-Asp in either the absence (solid line) or presence (dotted line) of NFA (300 μM) at normal [Cl^-] (103 mM) (Fig. 6A-1) and low [Cl^-] (30 mM) (Fig. 6B-1). At low [Cl^-], the crossover potential shifted toward the more negative potential (from -61 mV to -115 mV) and the sub-E_{rev} also shifted toward the more negative membrane potential. The average shift of the sub-E_{rev} gated by L-Asp was 94.9 ± 6.7 mV per 10-fold change in [Cl^-] (n=4) (Fig. 6C), indicating that Cl^- contributes to the L-Asp-gated NFA-induced conductance. Regarding L-Glu currents, no changes were observed in the crossover potential at low [Cl^-] (Figs. 7A-1, B-1) and a small shift of the sub-E_{rev} gated by L-Glu occurred at low [Cl^-] (Figs. 7A-2, B-2). The average shift of the sub-E_{rev} gated by L-Glu was 1.9 ± 8.1 mV per 10-fold change in [Cl^-] (n=4) (Fig. 7C), indicating that little contribution of Cl^- to the L-Glu-gated NFA-induced conductance. The significant difference in the additional Cl^- conductance between the L-Asp current and L-Glu current (Student's t-test, $p<0.05$) suggests that mechanisms for the modulation of EAAT1 currents by NFA is substrate-dependent.

DISCUSSION

In this study, we observed that the additional conductances

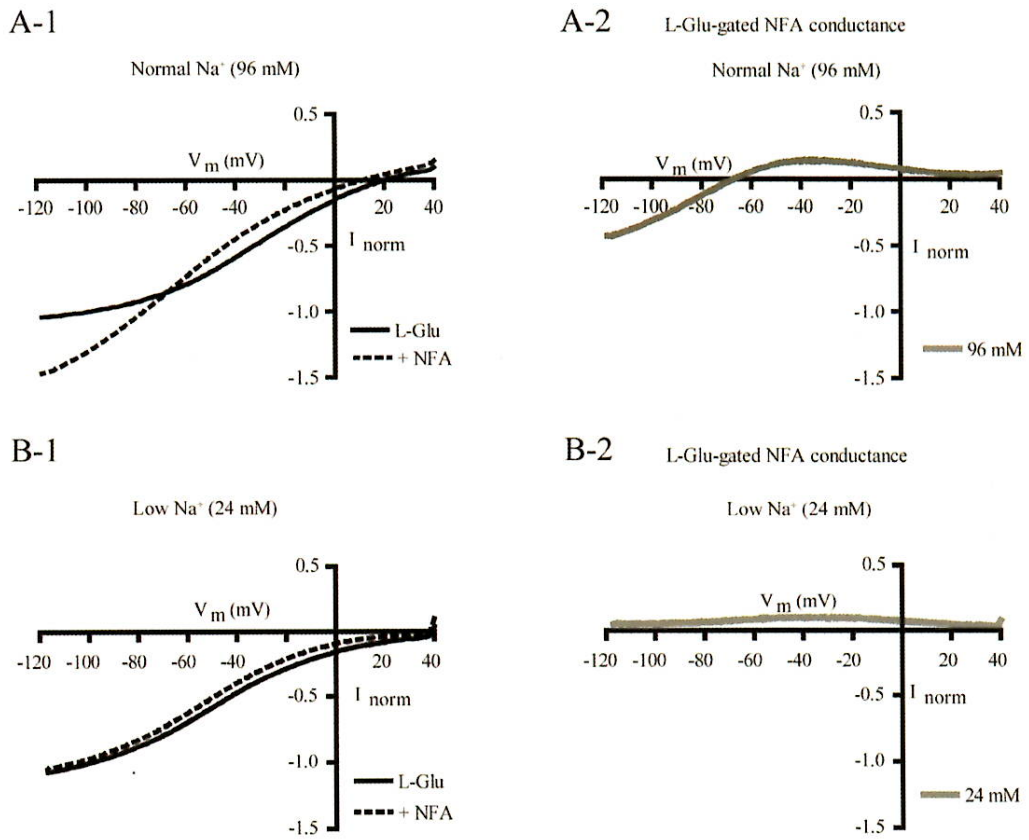

Fig. 5. Influence of Extracellular [Na^+] on L-Glu-Gated NFA-Induced Conductance and the L-Glu Currents in Either the Absence or Presence of NFA

A-1 and B-1: Average current–voltage relationships for L-Glu (30 μM) in either the absence (solid line) or presence (dotted line) of NFA (300 μM) at normal [Na^+] (96 mM) (A-1) and low [Na^+] (24 mM) (B-1). A-2 and B-2: Average current–voltage relationships for the L-Glu-gated NFA-induced conductance at normal [Na^+] (96 mM) (A-2) and low [Na^+] (24 mM) (B-2). The average shift of the sub-E_{rev} gated by L-Glu was 7.8±2.2 mV (n=3) per 10-fold change in [Na^+], which was statistically insignificant compared with that by L-Asp. Each point represents the mean from 5 oocytes.

of EAAT1 were activated when substrates were transported in the presence of NFA. Furthermore, the ionic contribution to the additional conductances is substrate dependent. To our knowledge, this is the first report showing the existence of additional conductances of EAAT1.

Poulsen and Vandenberg reported that NFA induced additional H^+ and Cl^- conductances in *Xenopus* oocytes expressing EAAT4, and these conductances were not thermodynamically coupled to the transport of substrates.[18] These conductances have been referred to as 'slippage.'[24] In our experiments using cultured astrocytes,[25] 300 μM of NFA significantly decreased the L-Glu uptake in cultured astrocytes (data not shown). Membrane potential of cultured astrocytes is approximately −74 mV.[26] Because the crossover potential of the L-Glu currents and NFA (300 μM)-gated L-Glu currents was −72.7±4.5 mV (n=12) in the present study, it is suggested that NFA-gated conductance observed here is not thermodynamically coupled to substrate transport, *i.e.*, NFA induces EAAT1 slippage as well. Transport experiments in voltage-clamped oocytes are necessary to confirm whether additional conductances in EAAT1 are not thermodynamically coupled to the substrate transport.

Sacher *et al.* presented a 'clutch' mechanism for slippage *via* the mammalian and yeast metal-ion transporter DCT1.[27] This mechanism could be explained in terms of two unique but interconnected ion pathways, one dominated by the ion utilized for driving the transport and the other by the transported metal ions. Loose coupling (namely clutching) between the driving force pathway and the metal ion transport pathway generates this observed slippage. Regarding EAAT1, in the presence of NFA, additional H^+ conductance may have arisen as a consequence of a subtle disruption to the ion binding sites, which compromises the coupling between the substrate transport pathway and the ion co-transport ($Na^+/H^+/K^+$) pathway. In support of this, a chimeric transporter generated with EAAT1 and EAAT2, whose junction site is in helical hairpin 2 and in close proximity to the substrate and Na^+ binding site, allows both Na^+ and K^+ to pass through the transporter in the absence of L-Glu.[28]

Interestingly, the ionic contribution is substrate-dependent, *i.e.*, the activation of additional H^+ conductance was involved in the modulation by NFA of both of L-Glu currents and L-Asp currents, whereas Cl^- was only involved in the modulation of L-Asp currents. Wadiche *et al.* reported that Cl^- permeation properties of EAAT1 were substrate-dependent, *i.e.*, the uncoupled Cl^- conductance per transport cycle gated by D-Asp was greater than that gated by L-Glu.[29] The mechanisms underlying the difference between L-Glu and L-Asp observed here may be related the one that causes the greater Cl^- by D-Asp. To elucidate the mechanisms, it is necessary to identify

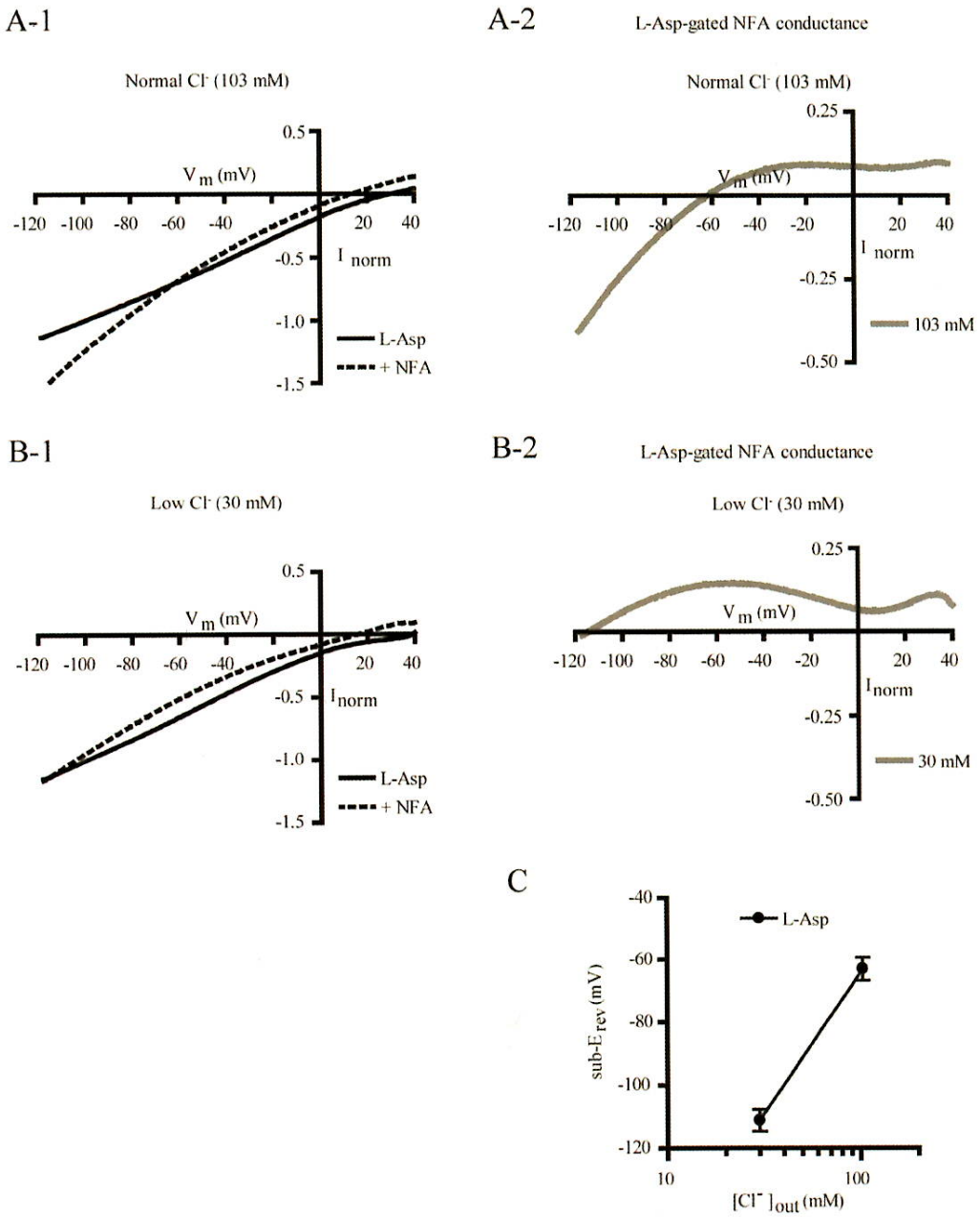

Fig. 6. Influence of Extracellular $[Cl^-]$ on L-Asp-Gated NFA-Induced Conductance and the L-Asp Currents in Either the Absence or Presence of NFA

The current–voltage relationships for the L-Asp current in either the absence or presence of NFA were examined under various extracellular $[Cl^-]$ by gluconate substitution. A-1 and B-1: Average current–voltage relationships for L-Asp (30 μM) in either the absence (solid line) or presence (dotted line) of NFA (300 μM) at normal $[Cl^-]$ (103 mM) (A-1) and low $[Cl^-]$ (30 mM) (B-1). A-2 and B-2: Average current–voltage relationships for the L-Asp-gated NFA-induced conductance at normal $[Cl^-]$ (103 mM) (A-2) and low $[Cl^-]$ (30 mM) (B-2). Each point represents the mean from 5 oocytes. C: Each point (filled circle) represents the mean sub-E_{rev} for L-Asp obtained in A-2 and B-2. Alterations in the extracellular Cl^- concentration caused average shifts of 94.9±6.7 mV per 10-fold change in $[Cl^-]$ (n=4) in the sub-E_{rev}.

the binding site of NFA on EAAT1, and the stoichiometric interaction among the substrates, EAAT1, and NFA.

Alterations in the glial intracellular pH can induce a variety of changes in cellular function, *e.g.*, ionic currents, gap junction conductance, and enzymatic activities.[30] For example, in Bergmann glial cells, which highly express EAAT1,[19,20] electrical coupling *via* gap junctions has been shown to be modulated by altering intracellular pH.[31] Activation of additional H^+ conductance by NFA could be related to the effects of the drug in altering intracellular pH.

In conclusion, we observed substrate-dependent mechanisms for the modulation of EAAT1 currents by NFA. Activation of additional H^+ conductance was involved in the NFA-induced modulation of EAAT1 currents induced by L-Asp and L-Glu. The Cl^- ion was only involved in the NFA-induced modulation of L-Asp currents.

Acknowledgments We would like to thank Dr. Y. Yasu-

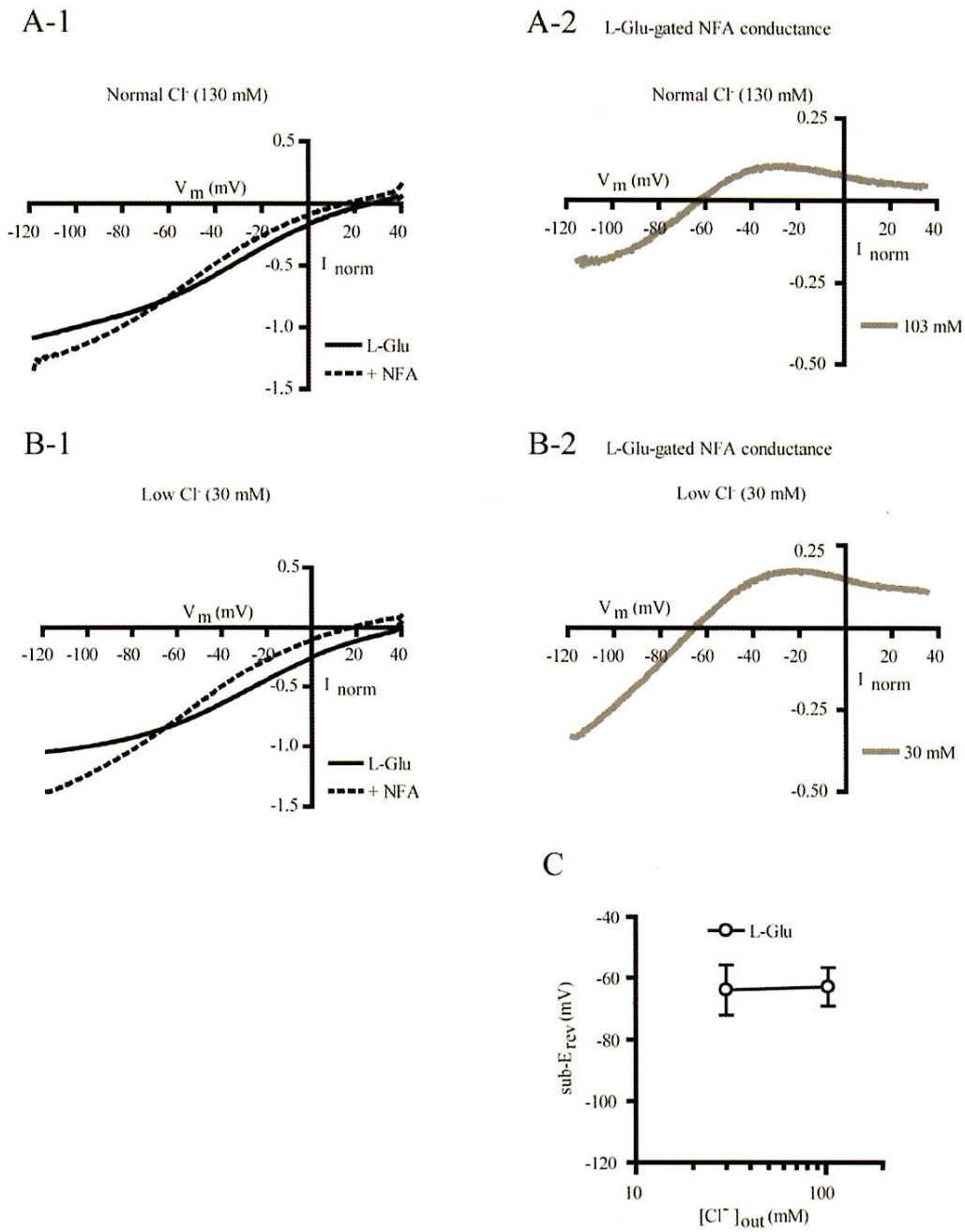

Fig. 7. Influence of Extracellular Cl^- on L-Glu-Gated NFA-Induced Conductance and the L-Glu Currents in Either the Absence or Presence of NFA

A-1 and B-1: Average current–voltage relationships for L-Glu (30 μM) in either the absence (solid line) or presence (dotted line) of NFA (300 μM) at normal [Cl^-] (103 mM) (A-1) and low [Cl^-] (30 mM) (B-1). A-2 and B-2: Average current–voltage relationships for the L-Glu-gated NFA-induced conductance at normal [Cl^-] (103 mM) (A-2) and low [Cl^-] (30 mM) (B-2). Each point represents the mean from 4 oocytes. C: Each point (open circle) represents the mean sub-E_{rev} for L-Glu obtained in A-2 and B-2. Alterations in the extracellular Cl^- concentrations caused average shifts of 1.9±8.1 mV per 10-fold change in [Cl^-] (n=4) in the sub-E_{rev}, which is significantly different from that of L-Asp (Student's t-test, $p<0.05$).

da-Kamatani and Dr. K. Shimamoto for providing the cDNA of EAAT1. We also thank Dr. T. Nakagawa and Dr. Y. Shigeri for their helpful suggestions. This work was partially supported by Grants-in-Aid for Young Scientists from the Ministry of Education, Culture, Sports, Science and Technology of Japan (KAKENHI 18700373, 21700422); Grant-in-Aid from the Food Safety Commission of Japan (No. 1003); the Program for the Promotion of Fundamental Studies in Health Sciences of NIBIO, Japan; a Health and Labour Science Research Grant for Research on Risks of Chemicals; and a Health and Labour Science Research Grant for Research on New Drug Development from MHLW, Japan; a Health and Labour Science Research Grant for Research on Risks of Chemicals from the MHLW, Japan; awarded to K.S. and a Health and Labour Science Research Grant for Research on New Drug Development from MHLW, Japan awarded to Y.S.

REFERENCES

1) Logan WJ, Snyder SH. Unique high affinity uptake systems for glycine, glutamic and aspartic acids in central nervous tissue of the rat. *Nature*, **234**, 297–299 (1971).
2) Zerangue N, Kavanaugh MP. Flux coupling in a neuronal glutamate transporter. *Nature*, **383**, 634–637 (1996).
3) Fairman WA, Vandenberg RJ, Arriza JL, Kavanaugh MP, Amara SG. An excitatory amino-acid transporter with properties of a ligand-gated chloride channel. *Nature*, **375**, 599–603 (1995).
4) Voutsinos-Porche B, Bonvento G, Tanaka K, Steiner P, Welker E, Chatton JY, Magistretti PJ, Pellerin L. Glial glutamate transporters mediate a functional metabolic crosstalk between neurons and astrocytes in the mouse developing cortex. *Neuron*, **37**, 275–286 (2003).
5) Veruki ML, Morkve SH, Hartveit E. Activation of a presynaptic glutamate transporter regulates synaptic transmission through electrical signaling. *Nat. Neurosci.*, **9**, 1388–1396 (2006).
6) Wersinger E, Schwab Y, Sahel JA, Rendon A, Pow DV, Picaud S, Roux MJ. The glutamate transporter EAAT5 works as a presynaptic receptor in mouse rod bipolar cells. *J. Physiol.*, **577**, 221–234 (2006).
7) White MM, Aylwin M. Niflumic and flufenamic acids are potent reversible blockers of Ca^{2+}-activated Cl^- channels in *Xenopus* oocytes. *Mol. Pharmacol.*, **37**, 720–724 (1990).
8) Scott-Ward TS, Li H, Schmidt A, Cai Z, Sheppard DN. Direct block of the cystic fibrosis transmembrane conductance regulator Cl^- channel by niflumic acid. *Mol. Membr. Biol.*, **21**, 27–38 (2004).
9) Ottolia M, Toro L. Potentiation of large conductance KCa channels by niflumic, flufenamic, and mefenamic acids. *Biophys. J.*, **67**, 2272–2279 (1994).
10) Busch AE, Herzer T, Wagner CA, Schmidt F, Raber G, Waldegger S, Lang F. Positive regulation by chloride channel blockers of IsK channels expressed in *Xenopus* oocytes. *Mol. Pharmacol.*, **46**, 750–753 (1994).
11) Wang HS, Dixon JE, McKinnon D. Unexpected and differential effects of Cl^- channel blockers on the Kv4.3 and Kv4.2 K^+ channels. Implications for the study of the I(to2) current. *Circ. Res.*, **81**, 711–718 (1997).
12) Malykhina AP, Shoeb F, Akbarali HI. Fenamate-induced enhancement of heterologously expressed HERG currents in *Xenopus* oocytes. *Eur. J. Pharmacol.*, **452**, 269–277 (2002).
13) Peretz A, Degani N, Nachman R, Uziyel Y, Gibor G, Shabat D, Attali B. Meclofenamic acid and diclofenac, novel templates of KCNQ2/Q3 potassium channel openers, depress cortical neuron activity and exhibit anticonvulsant properties. *Mol. Pharmacol.*, **67**, 1053–1066 (2005).
14) Fernandez D, Sargent J, Sachse FB, Sanguinetti MC. Structural basis for ether-a-go-go-related gene K^+ channel subtype-dependent activation by niflumic acid. *Mol. Pharmacol.*, **73**, 1159–1167 (2008).
15) Zwart R, Oortgiesen M, Vijverberg HP. Differential modulation of alpha 3 beta 2 and alpha 3 beta 4 neuronal nicotinic receptors expressed in *Xenopus* oocytes by flufenamic acid and niflumic acid. *J. Neurosci.*, **15**, 2168–2178 (1995).
16) Hu H, Tian J, Zhu Y, Wang C, Xiao R, Herz JM, Wood JD, Zhu MX. Activation of TRPA1 channels by fenamate nonsteroidal anti-inflammatory drugs. *Pflugers Arch.*, **459**, 579–592 (2010).
17) Furuta A, Rothstein JD, Martin LJ. Glutamate transporter protein subtypes are expressed differentially during rat CNS development. *J. Neurosci.*, **17**, 8363–8375 (1997).
18) Poulsen MV, Vandenberg RJ. Niflumic acid modulates uncoupled substrate-gated conductances in the human glutamate transporter EAAT4. *J. Physiol.*, **534**, 159–167 (2001).
19) Arriza JL, Fairman WA, Wadiche JI, Murdoch GH, Kavanaugh MP, Amara SG. Functional comparisons of three glutamate transporter subtypes cloned from human motor cortex. *J. Neurosci.*, **14**, 5559–5569 (1994).
20) Chaudhry FA, Lehre KP, van Lookeren Campagne M, Ottersen OP, Danbolt NC, Storm-Mathisen J. Glutamate transporters in glial plasma membranes: highly differentiated localizations revealed by quantitative ultrastructural immunocytochemistry. *Neuron*, **15**, 711–720 (1995).
21) Takahashi K, Ishii-Nozawa R, Takeuchi K, Nakazawa K, Sato K. Two non-steroidal anti-inflammatory drugs, niflumic acid and diclofenac, inhibit the human glutamate transporter EAAT1 through different mechanisms. *J. Pharmacol. Sci.*, **112**, 113–117 (2010).
22) DeCoursey TE, Cherny VV. Voltage-activated hydrogen ion currents. *J. Membr. Biol.*, **141**, 203–223 (1994).
23) Fairman WA, Sonders MS, Murdoch GH, Amara SG. Arachidonic acid elicits a substrate-gated proton current associated with the glutamate transporter EAAT4. *Nat. Neurosci.*, **1**, 105–113 (1998).
24) Vandenberg RJ, Huang S, Ryan RM. Slips, leaks and channels in glutamate transporters. *Channels* (Austin), **2**, 51–58 (2008).
25) Sato K, Matsuki N, Ohno Y, Nakazawa K. Estrogens inhibit L-glutamate uptake activity of astrocytes *via* membrane estrogen receptor alpha. *J. Neurochem.*, **86**, 1498–1505 (2003).
26) Nowak L, Ascher P, Berwald-Netter Y. Ionic channels in mouse astrocytes in culture. *J. Neurosci.*, **7**, 101–109 (1987).
27) Sacher A, Cohen A, Nelson N. Properties of the mammalian and yeast metal-ion transporters DCT1 and Smf1p expressed in *Xenopus laevis* oocytes. *J. Exp. Biol.*, **204**, 1053–1061 (2001).
28) Vandenberg RJ, Arriza JL, Amara SG, Kavanaugh MP. Constitutive ion fluxes and substrate binding domains of human glutamate transporters. *J. Biol. Chem.*, **270**, 17668–17671 (1995).
29) Wadiche JI, Amara SG, Kavanaugh MP. Ion fluxes associated with excitatory amino acid transport. *Neuron*, **15**, 721–728 (1995).
30) Deitmer JW, Rose CR. pH regulation and proton signalling by glial cells. *Prog. Neurobiol.*, **48**, 73–103 (1996).
31) Muller T, Moller T, Neuhaus J, Kettenmann H. Electrical coupling among Bergmann glial cells and its modulation by glutamate receptor activation. *Glia*, **17**, 274–284 (1996).